Europe PMC Funders Group
Author Manuscript
Nat Chem Biol. Author manuscript; available in PMC 2015 June 01.

Published in final edited form as:
Nat Chem Biol. 2014 December ; 10(12): 1020–1027. doi:10.1038/nchembio.1680.

Digital switching in a biosensor circuit via programmable timing of gene availability

Nicolas Lapique[1] and **Yaakov Benenson**[1,*]

[1]Department of Biosystems Science and Engineering, Swiss Federal Institute of Technology (ETH) Zurich, Mattenstrasse 26, Basel 4058 Switzerland

Abstract

Transient delivery of gene circuits is required in many potential applications of synthetic biology, yet pre-steady-state processes that dominate this delivery route pose significant challenges for robust circuit deployment. Here we show that site-specific recombinases can rectify undesired effects by programmable timing of gene availability in multi-gene circuits. We exemplify the concept with a proportional sensor for endogenous microRNA and show dramatic reduction in its ground state leakage thanks to desynchronization of circuit's repressor components and their repression target. The new sensors display dynamic range of up to 1000-fold compared to 20-fold in the standard configuration. We applied the approach to classify cell types based on miRNA expression profile and measured > 200-fold output differential between positively- and negatively-identified cells. We also showed major improvement of specificity with cytotoxic output. Our study opens new venues in gene circuit design via judicious temporal control of circuits' genetic makeup.

Introduction

Many cellular pathways are controlled by external molecular inputs via natural biosensor molecules such as cell surface receptors and transcription factors[1]. Engineered biosensing circuits are likewise increasingly used in basic research[2,3], bioproduction[4] and medicine[5,6]. Research in synthetic biology has greatly expanded the repertoire of tools for biosensor engineering with the development of toggle switches[7,8], band-pass filters[9], open-loop sensors[10], riboswitches[11], time-delay circuits[12] and oscillators[13,14]. Perhaps the most basic mode of sensing is proportional sensing[15], where increasing levels of input signal elicit higher levels of sensor output. For inputs with natural repressor function such as small molecule inhibitors, miRNA or transcriptional repressors, proportional sensing can be implemented with a synthetic "double inversion" module capable of suppressing the output expression while being suppressed by the input[16-19] (Fig. 1a). A simple way to characterize

Users may view, print, copy, and download text and data-mine the content in such documents, for the purposes of academic research, subject always to the full Conditions of use:http://www.nature.com/authors/editorial_policies/license.html#terms

*To whom correspondence should be addressed: kobi.benenson@bsse.ethz.ch.

Author contributions: N.L. conceived of the project, designed experiments, performed all the experiments, analyzed data and wrote the paper. Y.B. conceived of and supervised the project, designed experiments, analyzed data and wrote the paper.

Competing financial interests: The results of this manuscript have been submitted as a priority filing to the European Patent Office.

Europe PMC Funders Author Manuscripts
Europe PMC Funders Author Manuscripts

Europe PMC Funders Author Manuscripts

Europe PMC Funders Author Manuscripts

a sensor is to measure its Off and On states in the absence and presence of an input, respectively. Large dynamic range, that is, On:Off ratio, with such sensors is achieved by exogenous ligand IPTG[17], but for endogenous miRNA inputs the range is more modest[18].

Some of the sensors' potential applications are in diagnostics and gene therapy[20]. These scenarios require transient delivery of sensor-encoding genes using physico-chemical methods or viral vectors[21]. During transient delivery, system behavior is dominated by pre-steady-state processes that take place as the delivered genes become expressed and their products start interacting with each other and with cellular components. A particular challenge in sensors based on a double-inversion module is the simultaneous expression of the repressor components and their target output gene. Because the output does not initially "experience" the repressor action due to the lack of the latter, its concentration overshoots early in the process (*i.e.*, a pulse is generated) even when the repressor is potent[22-24]. In addition, transient delivery causes variability in gene copy number between cells, resulting in large cell-to-cell variability of the On output, which is typically proportional to the copy number of the output-encoding gene unless special compensating mechanisms are put in place[25]. Thus, the Off state is the prime target for sensor optimization and the improvement of the dynamic range.

Output pulse is a weakness of the double-inversion strategy, because even transient output expression can have physiological effects and because a stable protein output may linger in the cell for a long time. Since the pulse results from simultaneous commencement of gene expression, it could be possible to address the problem by desynchronizing the production of the repressor and the output species and creating a "buffer"[26] of repressor early on. This can be achieved by temporal control of circuit's genes, for example, by providing the repressor genes before the output genes. However, the application-imposed constraint regarding autonomous delivery of all system components requires that whatever tool is used to control the timing, it must be itself delivered together with the rest of the system. Here we demonstrate how temporal control of the circuit components can be implemented with site-specific recombinase co-delivered with the sensor genes, leading to dramatic improvement in sensor operational parameters. In particular, we delayed the availability of the output components, leading to early accumulation of repressor molecules and almost undetectable leakage in the Off state with fluorescent output. We performed thorough mechanistic investigation of this strategy and showed excellent digital performance in cell classification task, as well as demonstrated that it greatly improved the selectivity of very sensitive downstream physiological actuator HSV-TK in combination with ganciclovir pro-drug.

Results

The cause of leakage in the sensor

Our previously reported double inversion module (Fig. 1b) features a gene that encodes constitutively-expressed rtTA activator and an rtTA-controlled gene coding for a LacI repressor and an intronic, engineered miRNA miR-FF4[18]. LacI and miR-FF4 repress the output gene transcriptionally and posttranscriptionally, respectively. Both rtTA and LacI transcripts contain tandem repeats of perfectly complementary targets of a miRNA input of interest. Thus in the absence of a miRNA input, highly-expressed rtTA induces both LacI

Europe PMC Funders Author Manuscripts

and miR-FF4, which in turn repress the output. When miRNA input of interest is highly expressed, rtTA is strongly knocked-down and thus LacI and miR-FF4 are not expressed in the first place. In addition, LacI is knocked-down separately by the same miRNA input. This sequence of events enables output expression from LacI-controlled promoter.

Previously, we observed sensor leakiness in the Off state, even when the overall dynamic range (On:Off) was high. Leakiness in the Off state, regardless of the dynamic range, is undesirable because downstream processes could be highly sensitive to low, transient amounts of output. We established a new assay system to study the causes for sensor leakiness and optimize its performance. The assay comprises HEK293 cells that naturally express only trace amounts of miR-21[18]. We used miR-21 sensor with DsRed fluorescent output, generating sensor On state by co-transfecting saturating levels (10 pmol) of miR-21 mimic into the cells (Supplementary Results, Supplementary Fig. 1a). To evaluate the Off state, we used similar molar amount of negative control miRNA mimic.

Using this assay, we performed time-course measurements of the sensor response in both On and Off states, using transient transfection. Sensor dynamics revealed that in both states, the early expressing cells displayed very similar kinetics in the first few hours (0-5 h) before progressively diverging (Figs. 1c,d, Supplementary Fig. 1b), with the Off output displaying the characteristic pulse kinetics. This observation was qualitatively consistent with earlier findings regarding the delay between the expression of a repressor protein[27] or a miRNA[28] and the response of their target. Mean intensity of output expression in output-positive cells in the Off state peaked around 5-6 hours. Thus we hypothesized that a delay of 6-10 hours in the output gene availability and the commencement of output gene expression might substantially reduce the leakage.

Introducing a delay in output availability

A number of approaches could be envisioned to delay output production[12,29]. While control over gene expression timing using transcriptional regulation is one option, the most drastic and at the same time, “clean” intervention would be to withhold the gene itself. This requires programmable, time-dependent modification in the circuit-encoding DNA that is best achieved through DNA-manipulating enzymes such as recombinases. Therefore we opted for a recombinase-driven inversion of the output-coding region relative to its promoter. A Cre/Lox recombination system was engineered to delay output production, utilizing the FLEx switch that exploits the dual inversion and excision activity of the recombinase[30]. Using two pairs of incompatible Lox recombination sites, the coding region of the output sequence is stably and irreversibly inverted after Cre-mediated recombination (Fig. 2a). In a “delayed” sensor, the standard output construct was replaced with a backward-facing DsRed coding region; a constitutive Cre expression cassette was included with other circuit components. The delay amounted to 6-8 hours (Fig. 2b). As a result, we observed dramatic effect on the sensor Off state (Figs. 2c-e), in which virtually all the fluorescent leakage was eliminated, while the On state was only moderately reduced. This reduction in the On state could be largely explained by incomplete inversion of the backward-facing output (Supplementary Fig. 2a,b). There was an overall improvement of about 30-fold in the dynamic range of the sensor as shown in Fig. 2c. We note parenthetically that cotransfection

Europe PMC Funders Author Manuscripts

Europe PMC Funders Author Manuscripts

of negative control mimic, which is the appropriate Off measurement while using miR-21 mimic, increased the Off state of the standard sensor and to a less extent in the delayed sensor. Yet even when the negative control mimic was withheld (blue curve in Fig. 2c), there was about an order of magnitude improvement in the Off state.

Control of the timing

We observed that higher plasmid amount accelerated the recombination (Supplementary Fig. 2c) and proceeded to investigate the effect of recombinase-encoding plasmid dosage on the leakage and the dynamic range of the sensor. The On signal (Fig. 3a, top panel) fits the Hill function with n=1 and apparent "EC_{50}" in the order of 2 ng regardless of the quantitation method (Supplementary Fig. 3). The Off output depended on the amount of recombinase in an almost linear fashion (Off ~ $[Cre]^{0.77}$) (Fig. 3a, middle panel), resulting in On:Off ratio at lower recombinase levels reaching >2000-fold (Fig. 3a, bottom panel). Following optimization, we decided to use 5 ng of the plasmid encoding EF1α–driven iCre gene in the experiments that follow, unless indicated otherwise. The reduction in the On state at low plasmid levels of recombinase-encoding construct could be explained by reduced cotransfection efficiency of the recombinase and its target. In order to modulate Cre expression without affecting cotransfection efficiency, we used an inducible promoter driven by an ET1 transactivator whose activity can be controlled by the antibiotic erythromycin[31] (Supplementary Fig. 4). Similarly to plasmid titration, modulation of Cre activity showed that the Off level increased with increased recombinase expression, but the On state was constant in the promoter activity range (Fig. 3b).

We also tested whether the Off state could be further improved with additional chemical-induced delay. We used a Cre recombinase with estrogen receptors (ER)[32] fused at its C- and N-termini. Cre translocation into the nucleus is enabled upon Tamoxifen addition, hence the recombination can only occur in the presence of this drug. We used high amount of the fusion protein and delayed its activity by withholding Tamoxifen. This experiment showed that the Off state was improved upon extended delay, leading to larger dynamic range. The On signal is largely constant, only slightly decreasing when the drug is added 24 hours after transfection, probably due to shorter time available for recombination (Fig. 3c).

An approach to extend the delay autonomously without reverting to chemical ligands is to build a recombination cascade. We used a second site-specific recombinase Flp and Flp-compatible FLEx cassette to flank the Cre gene (Fig. 3d, top panel). To increase cotransfection of both recombinases, high amount of Cre-expressing plasmid (25 ng) was used in the standard, delayed (Cre) and Flp-Cre strategies. In a side-by-side comparison there was a 10-fold improvement over using one recombinase with similar plasmid amount with the dynamic range of ~1,500. Fine-tuning is likely to improve the range.

Alternatives to recombinase-induced delay

The results in Fig. 3 unequivocally indicated that the improvement in the Off state was the direct consequence of the delay in output gene availability, and that the dynamic range of the sensor could be controlled by a variety of methods including Cre gene dosage, control of Cre gene expression, control of Cre protein translocation, or a recombination cascade. We

Europe PMC Funders Author Manuscripts

Europe PMC Funders Author Manuscripts

examined the possibility to establish similar delay without the recombinase by sequential physical delivery of circuit genetic components, namely by sequential transfection of the miR-21 targeted rtTA and LacI/miR-FF4 genes, followed by the output gene. Because the DNA transfected at each step is loaded in separate liposomes, DsRed output and AmCyan control (transfected together with rtTA and LacI/miR-FF4 genes) showed very low correlation compared to simultaneous transfection (Supplementary Fig. 5). This also explained poor output repression with sequential transfection setup, whose overall performance was greatly inferior to the Cre-induced delay, emphasizing the importance of simultaneous and correlated delivery of genetic components. An alternative approach to dynamic range improvement could be accelerated delivery of the repressor by adding siRNA equivalent of miR-FF4 to generate strong knockdown at time zero. Indeed, even low amount of siRNA-FF4 (0.5 pmol) strongly reduced leakage of standard sensor with a moderate reduction of the On state, leading to a better dynamic range (Supplementary Fig. 6). However, further increase in siRNA amount, while reducing the leakage, also reduced the On state by a similar fraction without big improvement in the On:Off ratio The On state in the standard sensor is achieved by knockdown of rtTA with miRNA input such that the repressors LacI and miR-FF4 are never present at high levels. With siRNA-FF4, a large amount of repressor is introduced in both Off and On input states and full dilution or degradation of this siRNA would be required for high On state.

To conclusively eliminate any alternative explanation for leakage suppression in the Off state, we performed two more control experiments. First, we evaluated whether the anti-sense DsRed transcripts generated from backward-facing output genes sequestered forward-facing output transcripts. However, we did not observe a discernible effect when compared to “stuffer” DNA (Supplementary Fig. 7). Second, we checked whether the effect could be attributed simply to the reduction of the output gene dosage relative to double-inversion module genes due to incomplete recombination. We measured sensor performance with different ratios of inverted and forward-facing output genes, in the absence of Cre recombinase. Data in Supplementary Fig. 8a-d showed that while the Off state improved when the forward-facing output was reduced, the On output was reduced comparably, leaving the On:Off ratio largely constant. Thus using the recombinase reduces the leakage in the Off state without concomitant decrease in the On state that is observed with alternative approaches (Supplementary Fig. 8e,f).

Functional dissection of sensor components

The cumulative evidence shown above strongly favored the hypothesis that the recombinase-induced delay enabled the double-inversion module to produce enough repressor molecules prior to the commencement of output expression, thus greatly reducing the leakage. Next we asked which molecular features of the double-inversion module contributed most to this phenomenon. The repressor is a combined transcriptional/post-transcriptional unit that uses LacI and an artificial spliced miRNA (miR-FF4), respectively. We already showed that siRNA-FF4 had very strong inhibitory effect of its own (Supplementary Fig. 6). We mutated either the LacI or the miR-FF4 component (Fig. 4a,b), confirmed their loss-of-function (Supplementary Fig. 9), and measured sensor performance in both standard and delayed configurations (Fig. 4c). The data showed that while LacI-miR-

Europe PMC Funders Author Manuscripts

Europe PMC Funders Author Manuscripts

FF4 combination was the best performer, the LacI mutant still generated most of the total repression capacity via miR-FF4. In the delayed configuration it exhibited a dynamic range of more than two orders of magnitude, and likewise in the standard setting the effect of LacI removal was relatively minor. On the other hand, removing miR-FF4 had a major detrimental effect on both delayed and standard architectures. This indicates that an efficient repressor is a necessary prerequisite for high dynamic range in both standard and delayed configurations.

In order to further improve our understanding of sensor mechanism, we removed the activator rtTA and replaced the TRE promoter of LacI-miR-FF4 construct with a constitutive CMV promoter (Supplementary Fig. 10). We conjectured that removing rtTA induction would accelerate the expression of LacI and miR-FF4, thus improving the Off state to the level observed otherwise with Cre-induced delay. However, we only found a two-fold reduction of the leakage relative to both “wild-type” and $LacI^{mut}$ standard sensors. The leakage was further reduced when CMV was replaced by stronger CAG promoter driving LacI-miR-FF4 (Supplementary Fig. 10). Yet in line with expectation, without upstream transcriptional activator the repressor module of the sensor remained active despite the knockdown by miR-21, and the On state stayed very low because miR-FF4 level was not affected by RNAi knockdown against LacI that occurred after the splicing of miR-FF4[33]. For the same reason, we expected that in LacI mutant, the On and the Off states would be identical. Interestingly, we observed weak but reproducible de-repression even when LacI was mutated. One explanation is that in dividing cells such as HEK, the strict separation between nucleus and cytoplasm is not maintained all the time and thus even unspliced LacI-miR-FF4 transcript could be targeted by miR-21. To summarize, compared to standard sensor the repression can be slightly improved without upstream transcriptional activator, but the latter is essential for the sensor de-repression to high On state. This is consistent with the finding that most of the repressing effect comes from miR-FF4, and the only way to reduce miR-FF4 levels using another miRNA is by targeting its transcriptional activator.

We next asked whether individual circuit building blocks could be exchanged. First, we replaced LacI-controlled CAGop promoter with CMV; second, we replaced the DsRed output gene with ZsYellow (Supplementary Fig. 11). In both of these modifications the delayed circuit showed large improvement in the Off state compared to the standard configuration, as expected. Replacing DsRed with ZsYellow did not affect the performance, suggesting that the sensor can be used to control different output genes. Sensor with CMV promoter showed poor performance, in large part due to lower knock-down efficiency by miR-FF4 consistent with our earlier observations[34].

Sensor utilization for cell classification

Cell classification[18], or precise cell targeting based on complex signatures of endogenous markers such as miRNAs, has emerged as a promising development in mammalian synthetic biology with possible applications ranging from cell reprogramming to selective therapeutic agents. Any circuit architecture intended for this task must operate robustly in different mammalian cell types. To validate our approach in this scenario, we used a simplified version of the published HeLa classifier[18] utilizing two HeLa-high sensors for miR-21 and a

Europe PMC Funders Author Manuscripts

Europe PMC Funders Author Manuscripts

composite marker miR-17-30a, computing the logic AND gate "(miR-21) AND (miR-17-30a)". We first tested the miR-21 sensor alone, together with On and Off constitutive controls (Fig. 5a). In HeLa cells with EF1α–driven Cre (Fig. 5b, left), the basic recombination efficiency of the inverted output was poor (~35% relative to forward-facing constitutive On control, Fig. 5c, left). Therefore the expression level of the delayed miR-21 sensor in HeLa cells was also impaired (Fig. 5c, left and Supplementary Fig. 12), even though we still observed improved output ratio between HEK293 and HeLa cells. The reason for this could be poor cotransfection in HeLa, given the low molar ratio of EF1α–iCre cassette to output. To increase the amount of Cre plasmid without increasing recombinase levels, we exchanged the strong EF1α promoter with a weaker promoter SV40 (Fig. 5b, middle panel). SV40-iCre cassette was used in 1:2 molar ratio to the output plasmid, enabling much better signal recovery in HeLa cells (Fig. 5c, middle panel, and Supplementary Fig. 12). In addition, with this new setup the leakage in HEK293 cells was even lower than with EF1α–iCre cassette, resulting in about 400-fold differential expression between HEK293 and HeLa. In order to eliminate the consequences of imperfect Cre plasmid cotransfection, we embedded the SV40-iCre expression cassette and the output gene on the same plasmid (Fig. 5b, right panel). Mammalian promoter could have basal activity in prokaryotic cells[35], thus in order to avoid recombination during plasmid amplification in *E. Coli*, an intron was placed in the coding sequence of the recombinase. Interestingly, this configuration improved sensor performance even without delay (Fig. 5c, right panel, and Supplementary Fig. 12), via slight reduction of leakage in HEK293 and improvement in the On state in HeLa cells. The delayed miR-21 sensor using a single backbone gave the highest HeLa:HEK293 output ratio of about 500-fold; therefore this configuration was tested in the extended AND gate classifier circuit configuration. In this latter case (Fig. 5d and Supplementary Fig. 13), we observed excellent output ratio of about 250-fold between the cell lines with the delayed sensor. Thanks to the same-backbone configuration, the loss of circuit output in HeLa cells due to incomplete recombination was only about 10%.

Control of highly-potent physiological output

Lastly, we tested the ability of the delayed sensor to selectively cause cell death in the presence of high miR-21 levels, with the fluorescent output gene replaced by the gene encoding thymidine kinase from Herpes Simplex Virus (HSV-TK). This enzyme can induce cytotoxicity when acting on a prodrug Ganciclovir; the phosphorylated prodrug can be toxic to the cell expressing the enzyme as well as to bystander cells[36]. The combination of enzymatic actuation with bystander effect is a very sensitive reporter of leakage and we measured cytotoxicity using the total number of surviving cells. Cells viability was measured with live cells staining reagent Calcein AM and live cells numbers were measured by flow cytometry (See Materials and Methods). First, we tested miR-21 sensor in the standard and delayed configurations with miR-21 mimics in HEK293 cells (Fig. 6a and Supplementary Fig. 14). We used the exact same configuration (plasmid amounts, cell numbers and growth conditions) as for the fluorescent output, except the time between the transfection and the measurement was extended from 3 days to 5 days to allow the manifestation of cytotoxic effect. Using standard miR-21 sensor configuration, the cytotoxicity on the whole population level was strong and On (miR-21^{POS}) and Off (miR-21^{NEG}) states were very similar (Fig. 6a and Supplementary Fig. 14, standard

Europe PMC Funders Author Manuscripts

Europe PMC Funders Author Manuscripts

configuration). The cytotoxicity observed with constitutive expression of inverted HSV-TK + Cre was less drastic than with forward-facing TK but it still displays killing efficiency of 92%. With delayed miR-21 sensor, we could observe an expected trend, with most cells surviving in the Off state compare to the On state (Fig. 6a and Supplementary Fig. 14, delayed configuration). While the numbers are not perfect and the variability is high, there was dramatic improvement over the standard configuration.

Next, we attempted to translate differential expression of fluorescent output to selective cytotoxicity in different cell lines. We first tried to utilize the HEK293-HeLa combination, but HSV-TK failed to show toxic effect on HeLa cells presumably due to a poor bystander effect in this cell line[37]. Thus we looked into a few other cancer cell lines, namely HCT-116 and HuH-7, both expressing high levels of miR-21. We first tested the fluorescent sensor using SV40-iCre split plasmid configuration. Both cell lines showed high output compared to HEK293 cells (Supplementary Fig. 15). Preliminary tests showed 50% killing of HuH-7 cells and 80% killing of HCT-116 cells by constitutive HSV-TK (data not shown), consistent with cytotoxicity found in literature[38,39]; thus we chose HCT-116 cells for comparison with HEK293 cells (Fig. 6b and Supplementary Fig. 16). With standard sensor, different configurations generated similar levels of toxicity. Delayed miR-21 sensor in HCT-116 cells displayed similar toxicity as the constitutive HSV-TK expressed without delay, meaning that the sensor utilized most of its potential. Interestingly, the delayed constitutive Off sensor in HEK293 cells leads to almost complete cell survival, while miR-21 sensor shows some toxicity. This could be in fact due to very low background expression of miR-21 in HEK293[18]. In summary, only the delayed sensor showed selective actuation with this highly potent output.

Discussion

Our study showcases a novel strategy to dramatically improve the digital behavior of synthetic circuits by judicious recombinase-driven activation of various circuit genes at the appropriate time. In the particular sensor circuit described here, the strategy allows to dispense with some of the original circuit building blocks (i.e., LacI repressor) and still get much-improved performance. This greatly facilitates scaling such sensors to larger networks and reduces their DNA payload, opening new venues in biosensing and bio-actuation. There is a fixed size cost of a Cre expression cassette; however, the recombinase can be applied simultaneously to multiple miRNA-only switches that are themselves very compact.

Recombinases have been used to control gene expression in genetic engineering applications[40,41] and more recently, in biological computing circuits[42] to implement state machines[43], counters[44] and sequential logic[45,46]. Our report highlights additional dimension of recombinase utilization in synthetic circuits, namely their use to control the genetic makeup of the circuit in time-dependent fashion. Extension of this approach is likely to open new avenues in synthetic biology research.

Our results demonstrate how temporal control of circuit components could be crucial in conjunction with highly potent physiological output such as HSV-TK. The leakage in the Off state with standard sensor resulted in toxicity levels similar to the On state due to

Europe PMC Funders Author Manuscripts

Europe PMC Funders Author Manuscripts

enzymatic signal amplification, while the delayed sensor largely eliminated this undesired outcome. Extremely tight control of individual nodes in a biological network is also a general prerequisite for preserving or amplifying the initial input information. Thus our approach could enable reliable control of gene expression in small-scale engineered genetic components with potent physiological outputs, as well as facilitate “digital” signal propagation in large synthetic interaction cascades.

Online Methods

Synthetic miRNAs

RNA mimic of human miR-21 and negative control miRNA were purchased from Dharmacon RNAi Technology (Thermo scientific). miR-21 mimic (cat # C-300492-03-0005) is double-stranded RNA that mimics the function of human miRNA-21 (MI0000077). Negative Control mimic (cat # CN-001000-01-05) is based on a mix of C. Elegans miRNA sequences.

Chemicals

Doxycycline hyclate was purchased from Sigma-Aldrich (Fluka; cat # 44577-5G) and stock solution of 10mg/ml was prepared in deionized water. Erythromycin was purchased from Sigma-Aldrich (Sigma; cat # E5389-1G) and stock solution of 10 mg/ml was prepared in 100% ethanol. Ganciclovir was purchased from Sigma-Aldrich (Sigma; cat # G2536) and stock solution of 2.6 mg/ml (10 mM) was prepared in 2 mM HCl solution in deionized water. Tamoxifen ((Z)-4-Hydroxytamoxifen) was purchased from Sigma-Aldrich (Sigma; cat # H7904-5MG) and Stock solution of 0.39mg/ml was prepared in 100% ethanol. Calcein AM was purchased from Life Technologies (cat# C3100MP) and tubes with 50 μg were resuspended in 50 μl of 100% DMSO (1mM solution).

Cell culture and transfection

HEK293 (293-H) cell line was purchased from Invitrogen (Cat # 11631-017). HEK293 cells were cultured in RPMI-1640 medium (GIBCO® Life Technologies; cat # A10491-01) supplemented with 10% FBS (Sigma), 0.045 g/mL of penicillin and 0.045 g/mL streptomycin at 37 °C, 100% humidity and 5% CO_2. Lipofectamine 2000 transfection reagent (Life Technologies) was used in HEK293 experiments. 1.5×10^5 HEK293 cells were seeded in 1 mL RPMI 1640 complete medium into each well of 12-well uncoated plastic plate (Thermo Scientific Nunc) and grown for ~24 h. 2.8 μL of Lipofectamine 2000 were added to each sample as described in the manual using Optimem (Life Technologies) to resuspend DNA (100 μL/sample) and incubation reagent (100 μL/sample). Medium was changed before transfection with doxycycline to a final dilution of 1 μg/mL. HeLa cell line was purchased from ATCC (cat #CCL-2). HeLa cells were cultures in DMEM medium (Life Technologies GIBCO; cat #11966-025) supplemented with 10% FBS (Sigma), 4.5 g D-Glucose/L, 1 mM non-essential amino acids (Life Technologies GIBCO; cat #11140-035 at 37 °C, 100% humidity and 5% CO_2. HuH-7 cells were purchased from the Health Science Research Resources bank of the Japan Health Sciences Foundation (Cat-# JCRB0403, Lot-# 07152011) and cultured at 37 °C, 5% CO2 in DMEM, low glucose, GlutaMAX (Life technologies, Cat #21885-025), supplemented with 10% FBS and 0.045 g/mL of penicillin

Europe PMC Funders Author Manuscripts

Europe PMC Funders Author Manuscripts

and 0.045 g/mL streptomycin. HCT-116 were purchased from the Deutsche Sammlung von Mikroorganismen und Zellkulturen (DSMZ) (cat # ACC581). HCT-116 cells were grown in the exact same conditions than HeLa (See above). Cell line comparison was performed in 24-well uncoated plastic plate (Thermo Scientific Nunc) following the same protocol than with 12-well with plasmid amounts and transfection reagent scaled down by a factor of two. 7.5×10^4 HEK293, 6×10^4 HeLa, 4×10^4 HuH-7 and 1.5×10^5 HCT-116 were seeded in 500 μL of their respective complete media into each well of 24-well uncoated plastic plate (Thermo Scientific Nunc), grown for ~24 h. 1.4 μL of Lipofectamine 2000 were added to each sample as described in the manual using Optimem (Life Technologies) to resuspend DNA (50 μL/sample) and incubation reagent (50 μL/sample). Medium was changed before transfection with doxycycline to a final dilution of 1 μg/mL. Specific plasmid compositions for transfections performed in this manuscript are summarized in Supplementary Tables 1-15. Transfected cells were incubated for 3 days before flow cytometry analysis. All reported data are averaged values of three to six biological replicas. The error bars represent +/− one standard deviation.

Flow cytometry measurements

All samples were measured ~72 hours after transfection (or 5 days for cell viability assay) with Fortessa flow analyzers (BD Biosciences). DsRed was measured using 561 nm Laser, a 600 nm Longpass filter and a 610/20 emission filter with a PMT at 280V. AmCyan and Cerulean were measured using 445 nm Laser and 473/10 emission filter with a PMT at 280V. ZsYellow was measured using 480 nm Laser, a 505 Longpass filter and a 542/27 emission filter with a PMT at 220V. The improvement of the delayed sensor over standard architecture is not sensitive to specific PMT values in the DsRed channel as shown in Supplementary Fig. 17.

Delayed Cre Translocation

Experiments shown in Fig. 3c were performed as follows: 44 μl of Tamoxifen stock solution (0.39 mg/ml) were added to 4 ml of complete RPMI 1640 medium and 110 μl of the mixture were added into specific well in the 12-well plate at the time specified in the figure. After addition of the drug, the concentration of Tamoxifen in the well is 0.39 μg/ml, which is optimal to promote full translocation of the recombinase.

Fluorescent microscopy

Fluorescent images were acquired before flow cytometry measurements by an inverted Fluorescent Microscope (Nikon Eclipse Ti) using a Fiber Illuminator (Nikon Intensilight C-HGFI), optimized optical filtersets (Semrock) and a Digital Camera System (Hammamatsu, ORCA R2). Calcein AM was measured with the filter combination YFP HC (HC 500/24, HC 542/27, BS 520) with an exposure time of 300 ms. DsRed was measured with the filter combination TxRed HC (HC 624/40, HC 562/40, BS 593) with an exposure time of 1 sec. AmCyan was measured with the filter combination CFP HC (HC 438/24, HC 483/32, BS 458). Microscopy images were contrast-enhanced for better visualization by ImageJ software. Fig. 4b: in AmCyan images (16 bits), the intensity of LUT window was adjusted to 0-12000; in DsRed images (16 bits), the intensity of LUT window was adjusted to 1000-5500. Because DsRed channel had different background in HEK293 and HeLa,

Europe PMC Funders Author Manuscripts

Europe PMC Funders Author Manuscripts

background subtraction of 700 units was done in this channel in HeLa cells. In Fig. 5, Supplementary Fig. 15 and Supplementary Fig. 16, all images were first converted to 8 bits; in Calcein AM images (8 bits), the intensity of LUT widow was adjusted to 0-60 for HEK293 pictures and 0-50 for HCT-116 pictures.

Time course measurements

Transfections were done in 24-well uncoated plastic plate (Thermo Scientific Nunc) with seeding and transfection reagent scaled down by a factor of two (See Cell Culture and Transfection section). 21× master mix for each transfection was prepared and 1x of each master mix was added to each well individually. Each time course datapoint comes from a separate transfected well.

Data analysis

Scatter plots and bar charts in all the main and supplementary figures were generated as follows. Gating for %DsRed$^+$ was determined from AmCyan single color transfection with 99.9% DsRed$^+$ cells outside the gate. Gating for %AmCyan$^+$ was determined from DsRed single color transfection with 99.9% AmCyan$^+$ cells outside the gate. Gating examples are shown in Supplementary Fig. 18. For each sample, we calculated the frequency of DsRed-positive cells (%DsRed$^+$), the mean DsRed value in DsRed$^+$ cells, mean(DsRed$^+$), and the frequency of AmCyan positive cells (%AmCyan$^+$). The average signal per transfected cell, denoted as **DsRed/Cell, abs. u**. in the charts, was calculated as:

$$\frac{mean\left(DsRed^{+}\right) * \%DsRed^{+}}{\%AmCyan^{+}}$$

The average signal without normalization, denoted as **Σ DsRed a.u**. in the charts, was calculated as

$$mean\left(DsRed^{+}\right) * \%DsRed^{+}$$

The frequency of DsRed cells denoted as **DsRed$^+$/ AmCyan$^+$** in top row in Supplementary Fig. 3, was calculated as:

$$\frac{\%DsRed^{+}}{\%AmCyan^{+}}$$

The relative expression of DsRed signal denoted as **DsRed/Cell rel. u**. in the middle row in Supplementary Fig. 3, was calculated as:

$$\frac{mean\left(DsRed^{+}\right) * \%DsRed^{+}}{mean\left(AmCyan^{+}\right) * \%AmCyan^{+}}$$

Europe PMC Funders Author Manuscripts

Europe PMC Funders Author Manuscripts

Error propagation was used to estimate the error of the dynamic ranges and was calculated as:

$$\left\{\sqrt{\left(\frac{SD\,(dataset\quad 1)}{mean\,(dataset\quad 1)}\right)^2+\left(\frac{SD\,(dataset\quad 2)}{mean\,(dataset\quad 2)}\right)^2}\right\}*\frac{mean\,(dataset\quad 1)}{mean\,(dataset\quad 2)},$$

SD denotes standard deviation.

Cell viability assay

All experiments were performed in 24-well plates. The transfection protocol in HEK293 with miRNA mimics experiments was as described in Cell Culture and Transfection section. Medium was changed before transfection with doxycycline to a final dilution of 1 μg/mL and Ganciclovir to a final concentration of 100 μM. 5 days after transfection, the medium was replaced with a solution of PBS with 1 μM of Calcein AM. Cells were incubated in the dark for 30 min at 37 °C and imaged with fluorescent microscope. 1 drop/ml of calibration particles (Sphero™ BD Biosciences; cat # 559123) were added to 0.5% Trypsin-EDTA (GIBCO® Life Technologies; cat # 15400-054). Calcein AM solution was removed and 200 ul of trypsin with calibration particles was added to each well and incubated for 3 min at 37 °C. Cells were harvested, transferred to FACS tubes (Life Systems Design, Cat # 02-1412-000) and kept on ice before measurement by flow cytometry. Each tube was sampled for 30 seconds with Fortessa flow analyzer and cell number was inferred as follow. First, cells were gated using forward and side scatter channels, and in this gate cells positive for Calcein AM were counted. The volume of each sample measured by flow cytometry was normalized using the beads in solutions. The beads were identified with double gating, first selected on FSC and SSC channels, then gated using Red channel. Finally the number of $Calcein^{POS}$ cells was normalized to the number of beads in this sample to give a measure of cell number in the well. This measure was further normalized against the same measure obtained with the non-toxic control sensor transfected side-by-side (Supplementary Fig. 19a).

The experiments conducted in HEK293 and HCT-116 without mimics use the same transfection protocol as described in Cell Culture and Transfection section except than the same number (1×10^5) of HEK293 and HCT-116 cells was seeded 24 hours prior transfection. The cell viability assay was measured as described above. In addition we loaded some samples on an improved counting Neubauer chamber (cat# T729.1 Roth AG GMBH) and photographed with fluorescent microscope. The absolute number of cells per well, was determined from manual counting of Calcein-positive cells in at least $2{\times}1\ mm^2$ squares from the Neubauer chamber (Supplementary Fig. 19b). Counting from flow cytometry counting and Neubauer were extremely well correlated (Supplementary Fig. 19c). In Fig. 6, p-values were calculated with two-tailed t-test.

Europe PMC Funders Author Manuscripts

Europe PMC Funders Author Manuscripts

Plasmid DNA constructs

Standard molecular biology techniques were used. Oligonucleotides sequences used to prepare the plasmid DNA constructs are listed in Supplementary Table 16. All plasmids have been sequence-verified.

CAGop-Lox2272-LoxP-DsRed$_{Rev}$-Lox2272-LoxP-FF4 (pNL53)

DsRed was amplified from CAGop-DsRed-FF5-FF4 (pZ225) with PR1 and PR2. The PCR product replaced eGFP in CAG-Lox2272-LoxP-eGFP$_{Rev}$-Lox2272-LoxP (Addgene #28304) using XhoI and KpnI. CAG-Lox2272-LoxP-DsRed$_{Rev}$-Lox2272-LoxP was amplified with PR3 and PR4, and the PCR product replaced DsRed with Lox2272-LoxP-DsRed$_{Rev}$-Lox2272-LoxP in CAGop-DsRed-FF5-FF4 (pZ225) using NheI and HindII.

CAGop-Lox2272-DsRed-LoxP-FF4 (pNL75)

In vitro recombination of 250 ng of CAGop-Lox2272-LoxP-DsRed$_{Rev}$-Lox2272-LoxP-FF4 (pNL53), using 1 unit of Cre recombinase (NEB) during 30 min at 37°C.

TRE-LacI-T21-miR-FF4^{mut} (pNL73)

miR-FF4 in **TRE-LacI-T21-miR-FF4** (pZ224[18]) was replaced with mutant sequence (gBlock1 from IDT) using HindIII and SalI.

TRE-LacI^{mut}-miR-FF4 (pNL74)

Insertion of adenosine nucleotide after LacI start codon was done to produce a frameshift mutation. **TRE-LacI-T21-miR-FF4** (pZ224 in ref. 18) was amplified with phosphorylated PR5 and PR6, and PCR product was ligated.

TRE-LacI^{mut} -T21-miR-FF4^{mut} (pNL119)

TRE-LacI$_{mut}$-T21-miR-FF4 (pNL74) was digested with NheI and HindIII and LacI^{mut}-T21 fragment was inserted in TRE-LacI-T21-miR-FF4$_{mut}$ (pNL73) digested with the same enzymes.

CAGop-Lox2272-LoxP-ZsYellow$_{Rev}$-Lox2272-LoxP-FF4 (pNL98)

The construct was produced from three-parts assembly. CAGop-Lox2272-LoxP-DsRed$_{Rev}$-Lox2272-LoxP-FF4 (pNL53) was digested with XhoI and KpnI, ZsYellow was amplified from commercial plasmid pZsYellow1-N1 (BD Biosciences Clontech) with PR7 and PR8 and digested with XhoI and AscI, Lox2272-LoxP amplified from CAGop-Lox2272-LoxP-DsRed$_{Rev}$-Lox2272-LoxP-FF4 (pNL53) with PR9 and PR10 and digested with AscI and KpnI. The three fragments were ligated overnight at 4°C.

CAGop-Lox2272-ZsYellow-LoxP-FF4 (pNL101)

In vitro recombination of 250 ng of CAGop-Lox2272-LoxP-ZsYellow$_{Rev}$-Lox2272-LoxP-FF4 (pNL98), using 1 unit of Cre recombinase (NEB) during 30 min at 37°C.

Europe PMC Funders Author Manuscripts

Europe PMC Funders Author Manuscripts

EF1α–iCre (pEL0154)

Described previously[47].

CMV-Lox2272-LoxP-DsRed$_{Rev}$-Lox2272-LoxP-FF4 (pNL84)

CMV promoter from Advanced-tTA commercial plasmid (BD Biosciences Clonetech) was digested with SpeI and XbaI. It was used to replace CAGop promoter from CAGop-Lox2272-LoxP-DsRed$_{Rev}$-Lox2272-LoxP-FF4 (pNL53) digested with SpeI and NheI.

CMV-Lox2272-DsRed-LoxP-FF4 (pNL85)

CMV promoter from Advanced-tTA commercial plasmid (BD Biosciences Clonetech) was digested with SpeI and XbaI and replaced CAGop promoter from CAGop-Lox2272-DsRed-LoxP-FF4 (pNL75) digested with SpeI and NheI.

CMV-LacI-T21-miR-FF4 (pNL63)

LacI-T21-miR-FF4 was removed from TRE-LacI-T21-miR-FF4 (pZ224) with NheI and PciI. The fragment was used to exchange tTA in Advanced-tTA commercial plasmid (BD Biosciences Clontech) using XbaI and PciI.

CMV-LacI^{mut}-T21-miR-FF4 (pNL79)

LacI^{mut}-T21-miR-FF4 was digested from TRE-LacI^{mut}-T21-miR-FF4 (pNL74) with NheI and PciI. The fragment was used to replace tTA in Advanced-tTA commercial plasmid (BD Biosciences Clontech) using XbaI and PciI.

CMV-LacI-T21-miR-FF4^{mut} (pNL78)

LacI-T21-miR-FF4^{mut} was digested from TRE-LacI-T21-miR-FF4^{mut} (pNL73) with NheI and PciI. The fragment was used to exchange tTA in Advanced-tTA plasmid (BD Biosciences Clontech) using XbaI and PciI.

CMV-FRT-F3-iCre$_{rev}$-FRT-F3 (pNL114)

CMV-FRT-F3-Citrine$_{rev}$-miR-145-FRT-F3 (pEL0176) has been described previously[47]. iCre has been PCR amplified from EF1α-iCre using PR11 and PR12. The PCR product was used to replace Citrine-miR-145 in CMV-FRT-F3-Citrine$_{rev}$-miR-145-FRT-F3 using HindIII and SbfI.

EF1α-Cerulean (pKH024)

Cerulean was PCR amplified with PR13 and PR14 from CMV-Brainbow-2.1 R (Addgene plasmid #18723) and inserted in EF1α–eGFP (Addgene plasmid #11154) using EcoRI and EagI.

CAG-Cerulean (pNL111)

Cerulean was extracted from EF1α-Cerulean with EcoRI and BglII and exchange AmCyan in CAG-AmCyan digested with EcoRI and BamHI.

Europe PMC Funders Author Manuscripts

Europe PMC Funders Author Manuscripts

EF1α–FlpO (pEL0162)

Described previously[47].

CMV-ET1 (pEL0190)

Described previously[47].

ETR-iCre (pNL23)

P_{ETR8}-SEAP (pBP13[48]) was provided by Fussenegger lab. iCre was digested with EcoRI and NheI from Addgene plasmid #26745 and inserted in P_{ETR8}-SEAP digested with the same enzymes.

ETR-DsRed (pNL93)

P_{ETR8}-SEAP (pBP13[48]) was provided by Fussenegger lab. DsRed was digested with NheI and XmaI from CAGop-DsRed-FF4-FF5 (pZ223) and inserted in P_{ETR8}-SEAP between XbaI and AgeI

CAG-ERT2-iCRE-ERT2 (pNL125)

Addgene plasmid #13777

SV40-iCre (pNL127)

SV40 promoter was PCR amplified with PR15 and PR16 from sequence synthesized *de novo* by Genescript Inc. (last row of Supplementary Table 16) and inserted into EF1α–iCre (pEL154) using SalI and BamHI in order to exchange the promoter.

SV40-iCRE$_{exon1}$-intron-iCre$_{exon2}$ (pNL145)

5′ exon, the intron and fragment of the 3′ exon was synthesized *de novo* (gBlock2 from IDT DNA Inc.), PCR amplified with primer PR17 and PR18 and inserted in SV40-iCre (pNL127) using BamHI and BglII.

SV40-iCRE$_{exon1}$-intron-iCre$_{exon2}$-CAGop-Lox2272-LoxP-DsRed$_{Rev}$-Lox2272-LoxP-FF4 (pNL151)

PCR amplification of SV40-intron-iCRE in pNL145 with PR19 and PR20 and insertion of the amplicon in CAGop-Lox2272-LoxP-RevDsRed-Lox2272-LoxP (pNL53), digested with BsaI, using Gibson assembly[49].

SV40-iCre$_{exon1}$-intron-iCre$_{exon2}$-CAGop-Lox2272-DsRed-LoxP-FF4 (pNL152)

PCR amplification of SV40-intron-iCre in pNL145 with PR19 and PR20 and insertion of the amplicon in CAGop-Lox2272-DsRed-LoxP (pNL75) digested with BsaI using Gibson assembly[49].

CAGop-Lox2272-LoxP-HSV-TK$_{Rev}$-Lox2272-LoxP-FF4 (pNL199)

PCR amplification of Herpes simplex virus-Thymidine Kinase from Addgene plasmid #21911 (pNL157) using PR21 and PR22 primers. The amplicon replaced Reverse-ZsYellow

Europe PMC Funders Author Manuscripts

in CAGop-Lox2272-LoxP-Reverse-ZsYellow-Lox2272-LoxP-FF4 (pNL98) using XhoI and AscI.

CAGop-Lox2272-HSV-TK-LoxP-FF4 (pNL200)

PCR amplification of Herpes simplex virus-Thymidine Kinase from Addgene plasmid #21911 (pNL157) using PR21 and PR22 primers. The amplicon replaced ZsYellow in CAGop-Lox2272-ZsYellow-LoxP-FF4 (pNL101) using XhoI and AscI.

CAG-LacI-T21-miR-FF4 (pNL160)

Extract LacI-T21-miR-FF4 from TRE-LacI-T21-miR-FF4 (pZ224) using NheI and SalI and replace AmCyan in CAG-AmCyan (pZ183) using the same enzymes.

Plasmids reported previously[18]

CAG-AmCyan (pZ183), CAGop-DsRed-FF4-FF5 (pZ223), TRE-LacI-T21-miR-FF4 (pZ224), TRE-LacI-T17-T30a-miR-FF4 (pZ223), TRE-LacI-FF5-miR-FF4 (pZ225), CMV-rtTA-T21 (pZ090), CMV-rtTA-T17-T30a (pZ095), CMV-rtTA-FF5 (pZ091), pUBI-linker-NOS (pDT7004).

Supplementary Material

Refer to Web version on PubMed Central for supplementary material.

Acknowledgements

The work was funded the US National Institutes of Health and National Cancer Institute grant 5R01CA155320 and a European Research Council starting grant Cell Control. We wish to thank K. Hoelle and L. Prochazka for plasmids and Benenson lab members for discussions. We thank M. Dessing and V. Jaeggin for assistance with flow cytometry, and T. Horn for help with imaging. We thank Ryan Kellogg from S. Tay lab for help with viability assays.

References

1. Wodarz A, Nusse R. Mechanisms of Wnt signaling in development. Annual Review of Cell and Developmental Biology. 1998; 14:59–88.
2. Shimizu TS, Tu YH, Berg HC. A modular gradient-sensing network for chemotaxis in Escherichia coli revealed by responses to time-varying stimuli. Mol. Syst. Biol. 2010; 6:382. [PubMed: 20571531]
3. Mansfield JH, et al. MicroRNA-responsive ‘sensor’ transgenes uncover Hox-like and other developmentally regulated patterns of vertebrate microRNA expression. Nat. Genet. 2004; 36:1079–1083. [PubMed: 15361871]
4. Zhang FZ, Carothers JM, Keasling JD. Design of a dynamic sensor-regulator system for production of chemicals and fuels derived from fatty acids. Nat. Biotechnol. 2012; 30:354–359. [PubMed: 22446695]
5. Weber W, et al. A synthetic mammalian gene circuit reveals antituberculosis compounds. Proc. Natl. Acad. Sci. USA. 2008; 105:9994–9998. [PubMed: 18621677]
6. Callura JM, Dwyer DJ, Isaacs FJ, Cantor CR, Collins JJ. Tracking, tuning, and terminating microbial physiology using synthetic riboregulators. Proc. Natl. Acad. Sci. USA. 2010; 107:15898–15903. [PubMed: 20713708]
7. Gardner TS, Cantor CR, Collins JJ. Construction of a genetic toggle switch in Escherichia coli. Nature. 2000; 403:339–342. [PubMed: 10659857]

Europe PMC Funders Author Manuscripts

8. Egbert RG, Klavins E. Fine-tuning gene networks using simple sequence repeats. Proc. Natl. Acad. Sci. USA. 2012; 109:16817–16822. [PubMed: 22927382]
9. Basu S, Gerchman Y, Collins CH, Arnold FH, Weiss R. A synthetic multicellular system for programmed pattern formation. Nature. 2005; 434:1130–1134. [PubMed: 15858574]
10. de las Heras A, Carreno CA, Martinez-Garcia E, de Lorenzo V. Engineering input/output nodes in prokaryotic regulatory circuits. Fems Microbiology Reviews. 2010; 34:842–865. [PubMed: 20618867]
11. Liang JC, Chang AL, Kennedy AB, Smolke CD. A high-throughput, quantitative cell-based screen for efficient tailoring of RNA device activity. Nucleic Acids Res. 2012; 40:e154. [PubMed: 22810204]
12. Weber W, et al. A synthetic time-delay circuit in mammalian cells and mice. Proc. Natl. Acad. Sci. USA. 2007; 104:2643–2648. [PubMed: 17296937]
13. Elowitz MB, Leibler S. A synthetic oscillatory network of transcriptional regulators. Nature. 2000; 403:335–338. [PubMed: 10659856]
14. Prindle A, et al. A sensing array of radically coupled genetic 'biopixels'. Nature. 2011; 481:39–44. [PubMed: 22178928]
15. Tabor JJ, Levskaya A, Voigt CA. Multichromatic control of gene expression in Escherichia Coli. J. Mol. Biol. 2011; 405:315–324. [PubMed: 21035461]
16. Rinaudo K, et al. A universal RNAi-based logic evaluator that operates in mammalian cells. Nat. Biotechnol. 2007; 25:795–801. [PubMed: 17515909]
17. Deans TL, Cantor CR, Collins JJ. A tunable genetic switch based on RNAi and repressor proteins for regulating gene expression in mammalian cells. Cell. 2007; 130:363–372. [PubMed: 17662949]
18. Xie Z, Wroblewska L, Prochazka L, Weiss R, Benenson Y. Multi-input RNAi-based logic circuit for identification of specific cancer cells. Science. 2011; 333:1307–1311. [PubMed: 21885784]
19. Haynes KA, Ceroni F, Flicker D, Younger A, Silver PA. A sensitive switch for visualizing natural gene silencing in single cells. ACS Synthetic Biology. 2012; 1:99–106. [PubMed: 22530199]
20. Biffi A, et al. Lentiviral hematopoietic stem cell gene therapy benefits metachromatic leukodystrophy. Science. 2013; 341:1233158. [PubMed: 23845948]
21. Kota J, et al. Therapeutic microRNA delivery suppresses tumorigenesis in a murine liver cancer model. Cell. 2009; 137:1005–1017. [PubMed: 19524505]
22. Mangan S, Alon U. Structure and function of the feed-forward loop network motif. Proc. Natl. Acad. Sci. USA. 2003; 100:11980–11985. [PubMed: 14530388]
23. Basu S, Mehreja R, Thiberge S, Chen MT, Weiss R. Spatiotemporal control of gene expression with pulse-generating networks. Proc. Natl. Acad. Sci. USA. 2004; 101:6355–6360. [PubMed: 15096621]
24. Sontag ED. Remarks on feedforward circuits, adaptation, and pulse memory. IET Syst. Biol. 2010; 4:39–51. [PubMed: 20001091]
25. Bleris L, et al. Synthetic incoherent feedforward circuits show adaptation to the amount of their genetic template. Mol. Syst. Biol. 2011; 7:519. [PubMed: 21811230]
26. Weber W, Kramer BP, Fussenegger M. A genetic time-delay circuitry in mammalian cells. Biotechnology and Bioengineering. 2007; 98:894–902. [PubMed: 17461420]
27. Dunlop MJ, Cox RS, Levine JH, Murray RM, Elowitz MB. Regulatory activity revealed by dynamic correlations in gene expression noise. Nat. Genet. 2008; 40:1493–1498. [PubMed: 19029898]
28. Hausser J, et al. Timescales and bottlenecks in miRNA-dependent gene regulation. Mol. Syst. Biol. 2013; 9:711. [PubMed: 24301800]
29. Hooshangi S, Thiberge S, Weiss R. Ultrasensitivity and noise propagation in a synthetic transcriptional cascade. Proc. Natl. Acad. Sci. USA. 2005; 102:3581–3586. [PubMed: 15738412]
30. Schnutgen F, et al. A directional strategy for monitoring Cre-mediated recombination at the cellular level in the mouse. Nat. Biotechnol. 2003; 21:562–565. [PubMed: 12665802]
31. Weber W, et al. Macrolide-based transgene control in mammalian cells and mice. Nat. Biotechnol. 2002; 20:901–907. [PubMed: 12205509]

Europe PMC Funders Author Manuscripts

32. Matsuda T, Cepko CL. Controlled expression of transgenes introduced by in vivo electroporation. Proc. Natl. Acad. Sci. USA. 2007; 104:1027–1032. [PubMed: 17209010]
33. Singh J, Padgett RA. Rates of in situ transcription and splicing in large human genes. Nature Structural and Molecular Biology. 2009; 16:1128–1133.
34. Leisner M, Bleris L, Lohmueller J, Xie Z, Benenson Y. Rationally designed logic integration of regulatory signals in mammalian cells. Nat. Nanotechnol. 2010; 5:666–670. [PubMed: 20622866]
35. Kanegae Y, et al. High-level expression by tissue/cancer-specific promoter with strict specificity using a single-adenoviral vector. Nucleic Acids Res. 2011; 39:e7. [PubMed: 21051352]
36. Andrade-Rozental AF, et al. Gap junctions: the “kiss of death” and the “kiss of life”. Brain Research Reviews. 2000; 32:308–315. [PubMed: 10751679]
37. Mesnil M, Piccoli C, Tiraby G, Willecke K, Yamasaki H. Bystander killing of cancer cells by herpes simplex virus thymidine kinase gene is mediated by connexins. Proc. Natl. Acad. Sci. USA. 1996; 93:1831–1835. [PubMed: 8700844]
38. Mohr L, et al. Gene therapy of hepatocellular carcinoma in vitro and in vivo in nude mice by adenoviral transfer of the Escherichia coli purine nucleoside phosphorylase gene. Hepatology. 2000; 31:606–614. [PubMed: 10706550]
39. Mercer KE, Ahn CE, Coke A, Compadre CM, Drake RR. Mutation of herpesvirus thymidine kinase to generate ganciclovir-specific kinases for use in cancer gene therapies. Protein Engineering. 2002; 15:903–911. [PubMed: 12538910]
40. Backman K, Oconnor MJ, Maruya A, Erfle M. Use of synchronous site-specific recombination in vivo to regulate gene-expression. Bio-Technology. 1984; 2:1045–1049.
41. Dale EC, Ow DW. Gene-transfer with subsequent removal of the selection gene from the host genome. Proc. Natl. Acad. Sci. USA. 1991; 88:10558–10562. [PubMed: 1660141]
42. Benenson Y. Biomolecular computing systems: principles, progress and potential. Nat. Rev. Genet. 2012; 13:455–468. [PubMed: 22688678]
43. Ham TS, Lee SK, Keasling JD, Arkin AP. Design and construction of a double inversion recombination switch for heritable sequential genetic memory. PLoS One. 2008; 3:e2815. [PubMed: 18665232]
44. Friedland AE, et al. Synthetic gene networks that count. Science. 2009; 324:1199–1202. [PubMed: 19478183]
45. Siuti P, Yazbek J, Lu TK. Synthetic circuits integrating logic and memory in living cells. Nat. Biotechnol. 2013; 31:448–452. [PubMed: 23396014]
46. Bonnet J, Yin P, Ortiz ME, Subsoontorn P, Endy D. Amplifying genetic logic gates. Science. 2013; 340:599–603. [PubMed: 23539178]
47. Prochazka L, Angelici B, Haefliger B, Benenson Y. Highly modular bow-tie gene circuits with programmable dynamic behaviour. Nat. Communications. 2014; 5:4729.
48. Weber W, Kramer BP, Fux C, Keller B, Fussenegger M. Novel promoter/transactivator configurations for macrolide- and streptogramin-responsive transgene expression in mammalian cells. Journal of Gene Medicine. 2002; 4:676–686. [PubMed: 12439859]
49. Gibson DG, et al. Enzymatic assembly of DNA molecules up to several hundred kilobases. Nature Methods. 2009; 6:343–345. [PubMed: 19363495]

Europe PMC Funders Author Manuscripts

Europe PMC Funders Author Manuscripts

Europe PMC Funders Author Manuscripts

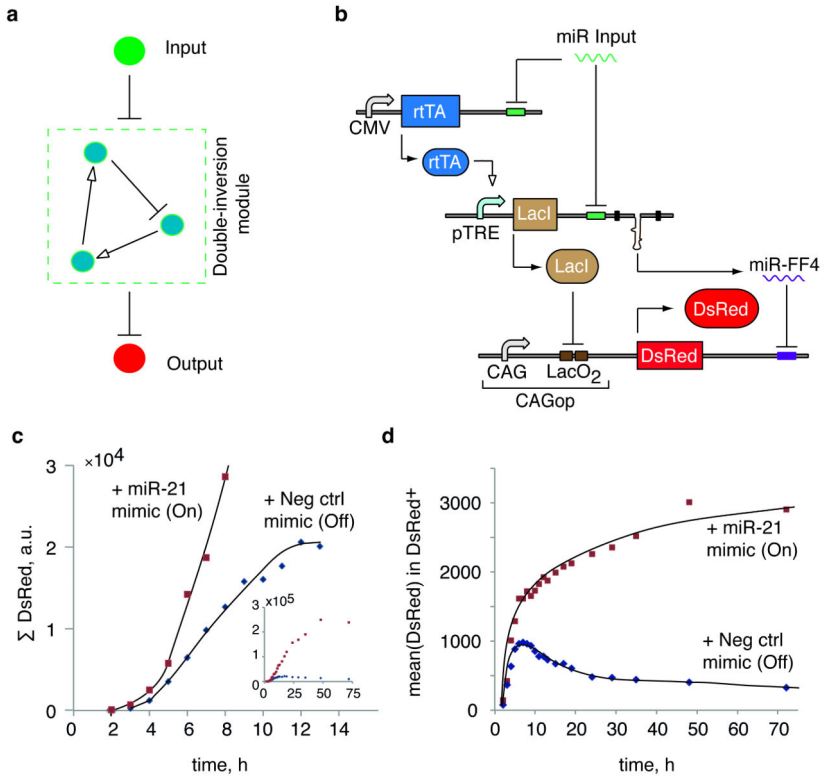

Figure 1. Source of leakage in the proportional sensor

a General layout of a proportional sensor for a negative regulator. An input elicits inhibitory effect on a double-inversion module, which in turn negatively regulates the output. **b** Circuit diagram of the proportional miRNA sensor, as previously reported[18]. Pointed arrows indicate activation while blunted arrows denote repression. Rectangles targeted by miRNA represent four identical sites for miR-21 and three identical sites for miR-FF4. **c** Total output signal shown as a function of time in both On (+ miR-21 mimics) and Off (+ Neg Ctrl mimics) sensor states. The signal is the sum of all DsRed intensities in DsRed-positive cells. The signal was not normalized because the expression of the transfection marker AmCyan showed very similar dynamics in all cases. Inset, time course over 72 hours. **d** Mean fluorescence of DsRed-expressing cells in Off (Blue) and On (Red) states, respectively, as a function of time. The curves were drawn manually to serve as guides.

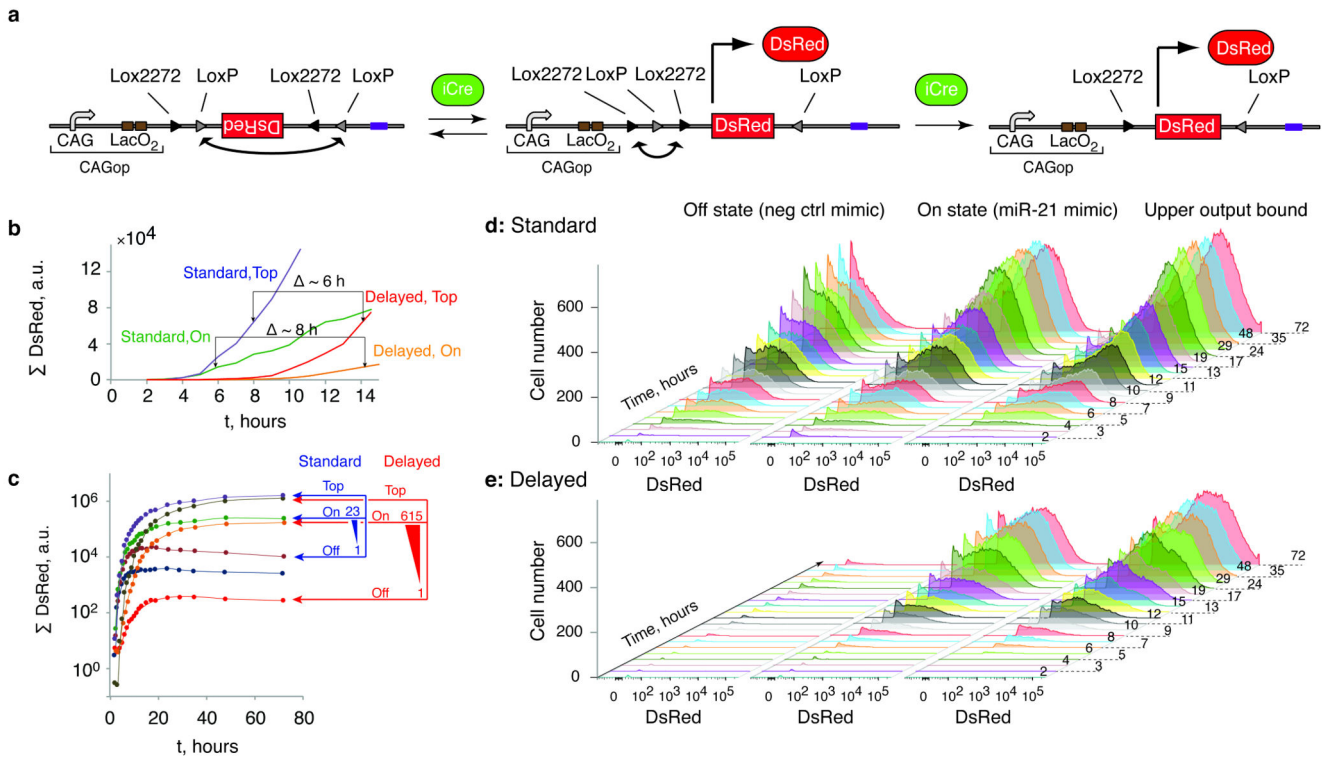

Figure 2. The effect of delayed output on sensor performance

a The principle behind the FLEx inversion system[30]. **b-e** Time course measurements of standard and delayed sensor architectures. **b** Time course of total output protein expression from the uncontrolled forward-facing output gene (Standard, Top, blue line) and delayed output expression from uncontrolled backward-facing output gene (Delayed, Top, red line), showing about a six-hour delay. Comparison of the On signal development in the standard (Standard, On, green line) and the delayed (Delayed, On, orange line) sensor displayed an 8-hour delay. Only the first 14 hours are shown. **c** Time course of total DsRed signal corresponding to the uncontrolled output gene (Top), miR-21 sensor in the presence of miR-21 mimic (On) and sensor in the presence of negative control mimic (Off), corresponding to both standard and delayed configurations as indicated in the chart, over 72 hours. The fold-ratios between the On and the Off signals are shown. The blue curve corresponds to the Off state of the standard sensor in the absence of any miRNA mimic (see main text). **d** Time-dependent histograms of DsRed output in the standard sensor configuration. Different setups are indicated on top. The label “Upper output bound” corresponds to DsRed expression from uncontrolled output gene (same as “Top” in **b** and **c**). **e** Time course measurements in the delayed configuration. The Off and On time series are as in **d**.

Europe PMC Funders Author Manuscripts
Europe PMC Funders Author Manuscripts

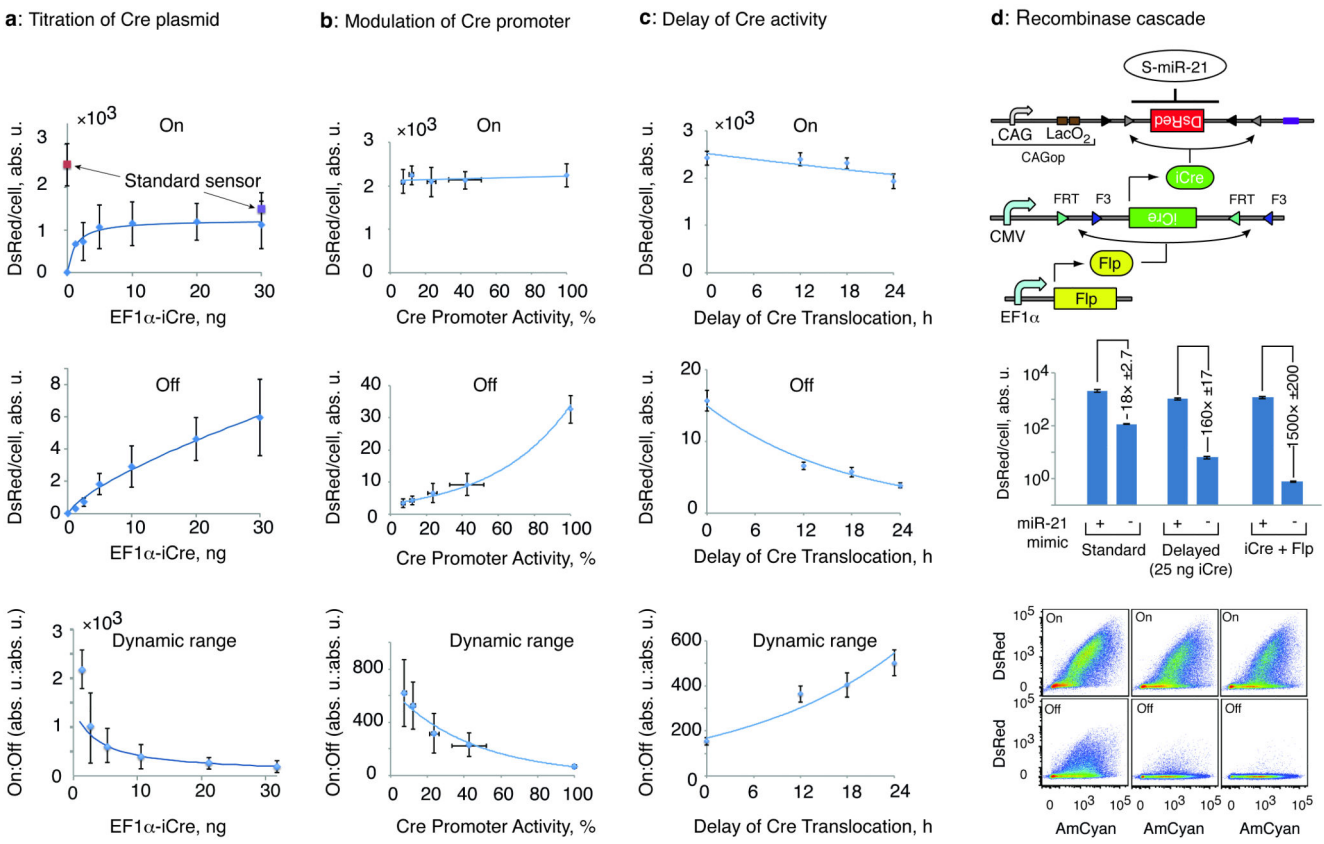

Figure 3. Control of the timing

a-c The top, the middle and the bottom charts rows correspond to On state, Off state and On:Off ratio, respectively. The On:Off curves are calculated by dividing the fitted curves of the On by the Off measurements. **a** Delayed sensor characterization as a function of Cre-expressing plasmid amount. The curves are fitted to Hill function with n = 1 (On states) and to power law (Off states). **b** Modulation of Cre expression with an inducible promoter. ETR-iCre activity was ascertained from ETR-DsRed reporter with various concentration of erythromycin (Supplementary Fig. 4). X-axis shows percentage of promoter activity relative to full activity in absence of Erythromycin. The curves are fitted to linear (On states) and exponential (Off states) regressions. **c** Chemical delay of ER2-Cre-ER2 translocation. X-axis shows the time (hours) between the transfection and the addition of Tamoxifen. The curves are fitted to linear (On states) and exponential (Off states) regressions. **d** Recombinase cascade eliminates the leakage. Sensor diagram is shown (left). The bar chart compares standard architecture with a Cre-only delayed architecture to a cascade system, with the representative flow cytometry scatter plots shown on the right. Error bars show ± standard deviation from at least three biological replicas.

Europe PMC Funders Author Manuscripts
Europe PMC Funders Author Manuscripts

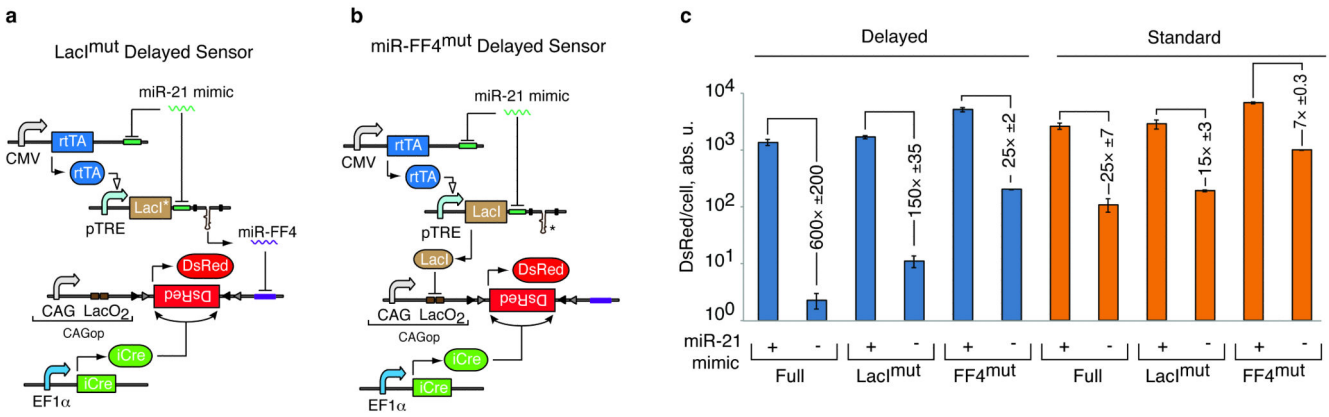

Figure 4. Component contribution to sensor performance

Circuit diagrams of miR-FF4 mutant sensor (**a**), LacI mutant sensor (**b**) and their relative performance (**c**). Asterisks indicate mutated components. Error bars show ± standard deviation from at least three biological replicas.

Europe PMC Funders Author Manuscripts
Europe PMC Funders Author Manuscripts

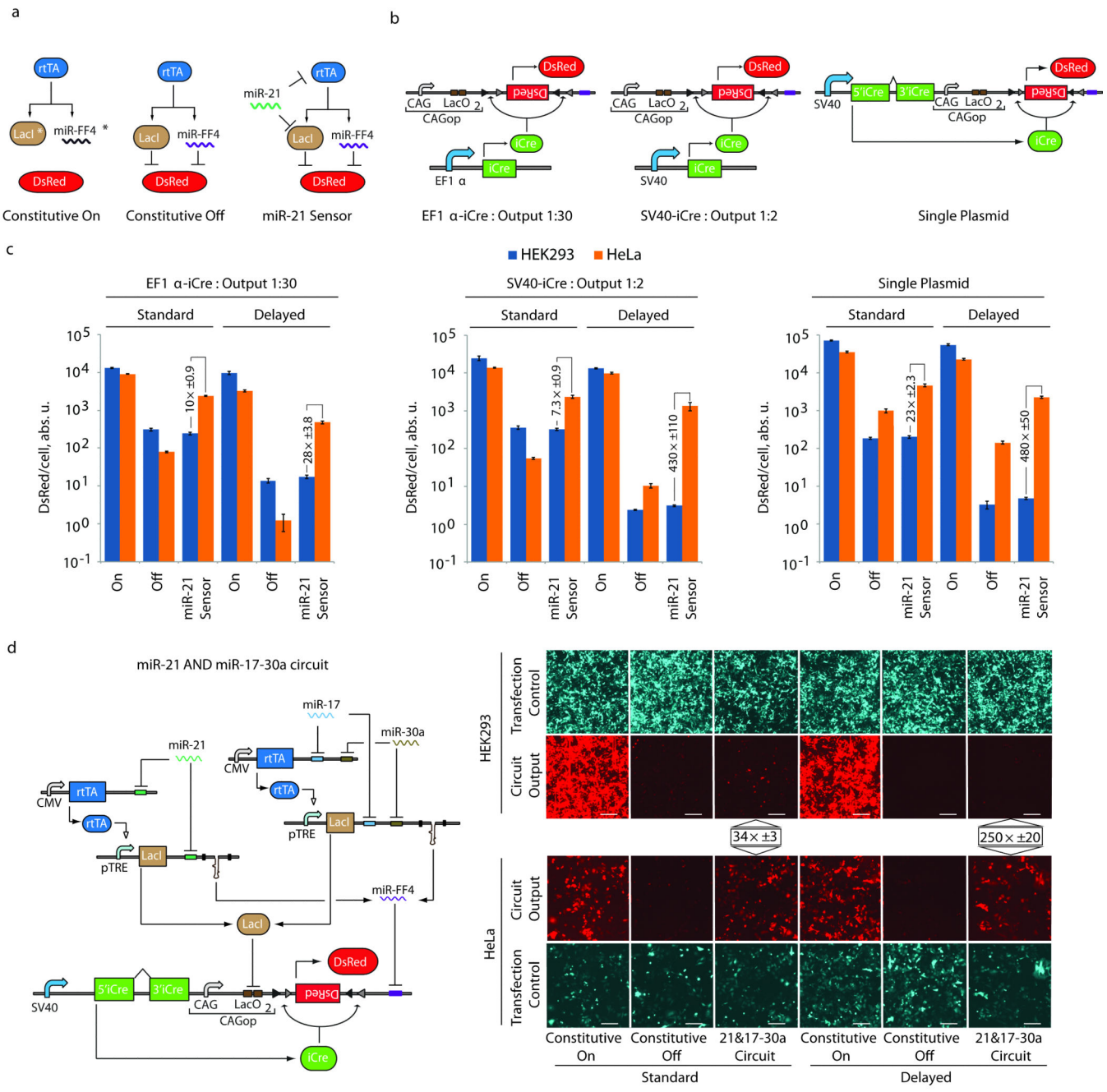

Figure 5. Cell type classification

Schematics of tested sensors and controls (**a**) and delayed output variants (**b**). **c** Output in HeLa cells relative to HEK293 cells. Each bar chart compares output intensity in HEK293 and HeLa cells using a particular output variant with three sensor variants (On, Off, and miR-21 sensor) in forward-facing and delayed configurations. Flow cytometry plots are shown in Supplementary Fig. 12. **d** A version of HeLa cell classifier encoding "(miR-21) AND (miR-17-30a)" logic gate. Delayed and standard circuits have the SV40-iCre cassette embedded on output plasmid. Representative microscopy snapshots show transfection control (Cyan pseudocolor) and circuit output (Red pseudocolor). Each panel compares

Europe PMC Funders Author Manuscripts
Europe PMC Funders Author Manuscripts

HEK293 with HeLa with three different circuit variants (On, Off, actual logic circuit) in standard and delayed configurations. Flow cytometry scatter plots are in Supplementary Fig. 13. Error bars show ± standard deviation using at least three biological replicas. Scale bars, 300 μm.

Europe PMC Funders Author Manuscripts

Europe PMC Funders Author Manuscripts

Europe PMC Funders Author Manuscripts

Europe PMC Funders Author Manuscripts

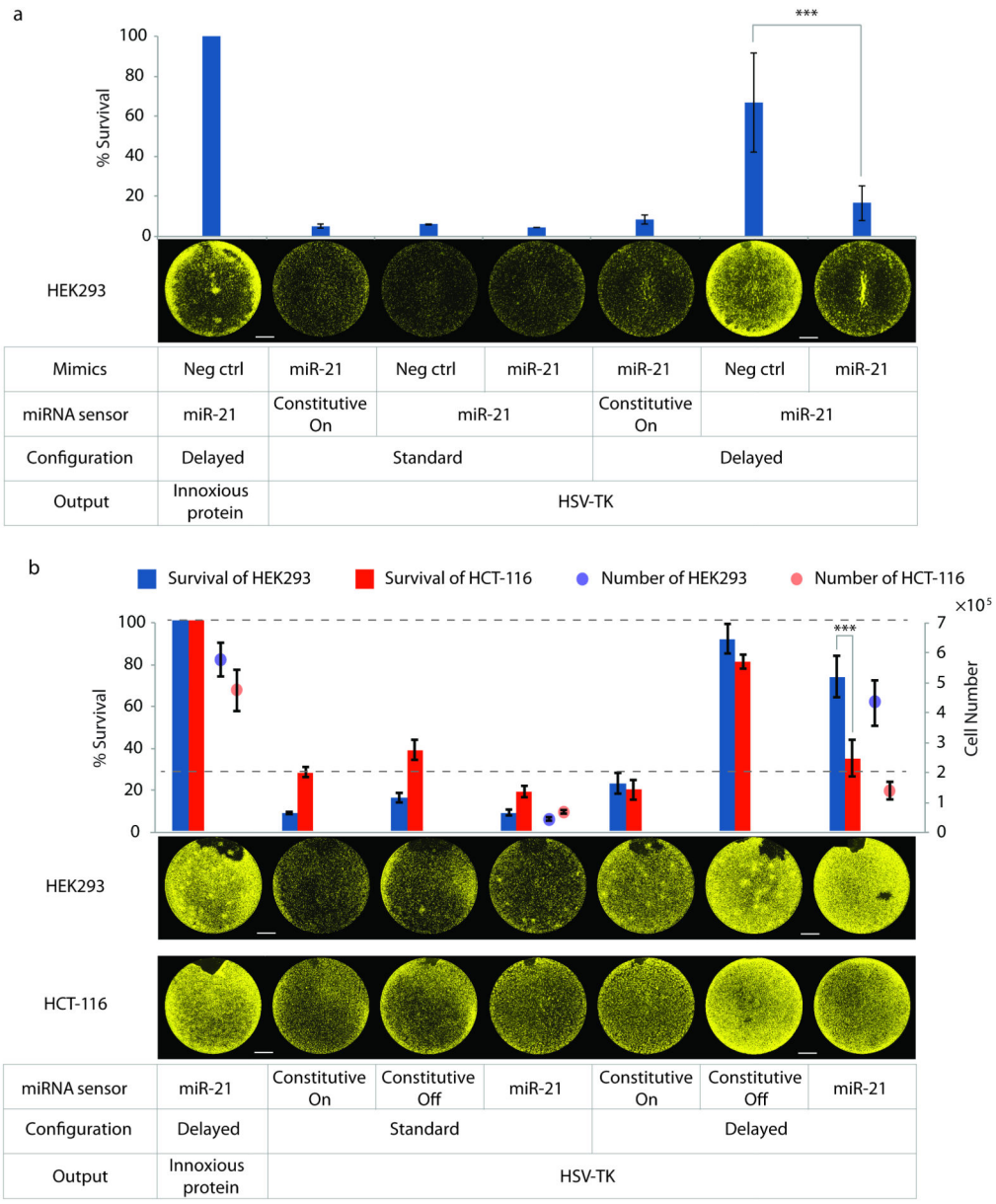

Figure 6. Selective cytotoxicity in HEK293 and HCT-116 cells with HSV-TK output

The bar charts show cell survival with the indicated circuit and miRNA mimics. Survival is the cell number percentage relative to the control well transfected side by side with non-toxic DsRed-producing sensor (Innoxious protein). For illustration, we show fluorescent images of entire wells stained with a dye for live cells (Calcein, AM). **Note** that due to high variability in the absolute staining intensity per cell (as opposed to the number of stained cells), the images cannot be used to make quantitative conclusions. The numbers are measured by flow cytometry and/or cell counting, see Online Methods. **a** Selective cytotoxicity in HEK293 cells elicited with miR-21 sensor in the presence of miR-21 (On state, cell death expected) or negative control mimics (Off state, cell survival expected). Constitutive On condition uses double-mutant LacI^{MUT}miR-FF4^{MUT} miR-21 sensor that

cannot repress HSV-TK. Individual replicates are shown in Supplementary Fig. 14. **b** Selective cytotoxicity in HEK293 and HCT-116 cells elicited by differential expression of endogenous miR-21 in these cell lines. Constitutive On condition uses double-mutant $LacI^{MUT}$miR-FF4^{MUT}, and constitutive Off uses a sensor with rtTA and LacI genes furnished with scrambled targets insensitive to miR-21. In addition, absolute numbers of HCT-116 and HEK-293 cells are shown (right axis) for the non-toxic control sensor without HSV-TK output, and miR-21 sensors with HSV-TK output. Individual replicates are in Supplementary Fig. 16. ***$p<0.0001$. Error bars show ± standard deviation using at least three biological replicas. Scale bars, 3 mm.

Europe PMC Funders Author Manuscripts

Europe PMC Funders Author Manuscripts